CHAPTER 13

Modified montmorillonite in photo-Fenton and adsorption processes

Lucas M. Guz, Melisa Olivelli, Rosa M. Torres Sánchez,
Gustavo Curutchet & Roberto J. Candal

13.1 INTRODUCTION

Nowadays environmental pollution is one of the major and more urgent problems to be resolved in the world. In particular, water contamination affects most of the planet being the situation more dramatic in the less developed countries. All the human activities from agriculture to the fabrication of sophisticated electronic equipment need water, generating enormous amounts of effluents that should be purified before being discharge to the environment. Biological water treatment is without doubts the most popular in the entire world because it is versatile, cheap and can be used in big or small cities and for several industries. However, human activity generates wastewaters containing soluble metals and/or synthetic organic compounds that are non-biodegradable or, unlike natural occurring compounds, extremely resistant to biodegradation by native microorganisms (Ali, 2010). Synthetic dyes belong to the group of poorly biodegradable compounds and approximately 20% of the synthesized dyes are discharged in aqueous effluents without any treatment (O Neill *et al.*, 1999). Synthetic dyes are made up of complex aromatic molecular structures purposely designed to resist the exposure to light, water, air, soap and oxidizing agents. Consequently, dyes are commonly resistant to conventional biological treatment and in particular to aerobic digestion (Asgher, 2012). Although anaerobic degradation of dyes is reported, toxic amines intermediates are usually produced as byproducts and the coupling of anaerobic with aerobic treatment is usually recommended (Hosseini Koupaie *et al.*, 2013; Singh, 2011).

Physicochemical water treatments that can be used to remove non-biodegradable compounds include adsorption, coagulation-flocculation, membrane filtration, ozonization and advanced oxidation, between others. The sorption methods are relatively fast, can be used to remove metals and organic compounds, and may be cheaper than others. However, they have the problem of the further elimination of the sorbed pollutant, which has to be treated as a dangerous waste. Other techniques (like membrane filtration or ozonization) require significant amount of electricity and the cost may be too high in regions were electricity is expensive. Advanced oxidation processes (AOPs) are an alternative that works well for the elimination of organics. The most used AOPs are Fenton like, photo-Fenton like and TiO_2-photocatalysis. The three processes have been used for the degradation of dyes; Fenton like and photo-Fenton like processes are being increasingly used in the treatment of industrial wastewater including colored waters (Bautista *et al.*, 2007; Lofrano *et al.*, 2007; Meriç et al., 2005). Although the Fenton reagent has been known for more than a century and is shown to be a powerful oxidant, the mechanism of the Fenton reaction is still under intense and controversial discussion. However, it is generally accepted that the reaction between H_2O_2 and Fe^{2+} in an acidic aqueous medium ($pH \leq 3$) produces $HO^{\bullet}$ radicals that act as non-selective oxidants that can degrade or even mineralize different types of organic substances. In a typical approach, four steps should be followed: pH adjustment to 2.8–3.0, oxidation reaction, neutralization, and coagulation. The process can be summarized as:

$$Fe^{2+} + H_2O_2 \rightarrow Fe^{3+} + HO^{-} + HO^{\bullet} \quad (13.1)$$

As iron (II) acts as a catalyst, it has to be regenerated, which seems to occur through the following scheme:

$$Fe^{3+} + H_2O_2 \leftrightarrow Fe\text{–}OOH^{2+} + H^+ \tag{13.2}$$

$$Fe\text{–}OOH^{2+} \rightarrow Fe^{2+} + HO_2^{\bullet -} \tag{13.3}$$

The photo-Fenton process produces more hydroxyl radicals in comparison to the conventional Fenton method, thus promoting the degradation of organic pollutants. The photo-Fenton reaction involves irradiation with UV light that significantly increases the rate of contaminant degradation by stimulating the reduction of Fe(III) to Fe(II). Further hydroxyl radicals may be produced via direct H_2O_2/UV photolysis (slow reaction, depending on the emission of the lamp) and the reaction of H_2O_2 with Fe^{2+} produced by photoreduction of Fe(III):

$$Fe(OH)^{2+} + h\nu \rightarrow Fe^{2+} + HO^{\bullet} \tag{13.4}$$

$$Fe^{2+} + H_2O_2 \rightarrow Fe(OH)^{2+} + HO^{\bullet} \tag{13.5}$$

The photoreduction of $Fe(OH)^{2+}$ takes place with wavelength of 360 nm (UVA radiation), meaning that solar light can be used as a irradiation source in photo-Fenton process (Herney-Ramirez *et al.*, 2010). The higher production of $HO^{\bullet}$ due to the combination of oxidants and metallic catalysts in the presence of UVA radiation, and the potential applicability of sunlight as UVA light source are some attractive advantages of this process (Pignatello *et al.*, 2006). The Fenton reagent usually incorporates Fe(II) as catalyst, but, in some cases, using only iron, it is not possible to remove all the intermediate compounds generated as a consequence of the partial oxidation of the pollutants (Primo *et al*., 2008). Other transition metals appear as an alternative to achieve higher mineralization efficiencies; these alternatives are the so-called Fenton like process. Copper undergoes Fenton and photo-Fenton type reactions and lead to the oxidation of several compounds (Anipsitakis and Dionysiou, 2004; Neamtu *et al.*, 2003; Shah *et al.*, 2003).

As mentioned before, the photo-Fenton reaction has been widely applied under homogeneous conditions. It is an effective method for the removal of a high variety of organic contaminants, with the advantages of working under simple operation conditions and the relatively low price and environmental impact of the oxidation reagents. However, this application has various serious disadvantages, for example, the formation of Fe-containing sludge and the low pH necessary for optimal performance. Besides, the catalytic activity of Fe(III) can be diminished by the presence of complexing agents able to form very stable coordination compounds. The use of supported catalysts has been reported as a solution to these problems (Herney-Ramirez *et al.*, 2010). Several alternatives were proposed as heterogeneous catalysts for Fenton process; bulk catalysts containing iron may be considered, as hematite, magnetite, goethite, etc. A different approach is the incorporation of iron into different supports as activated carbon (Dhaouadi and Adhoum, 2010), polymers (Lee *et al.*, 2010), zeolites (Idel-Aouad *et al.*, 2011), clays, etc. The use of clays as catalyst support for Fenton reaction has been recommended by several authors, with application in general wastewater treatment (Herney-Ramirez *et al.*, 2010) and especially in wastewaters containing different types of dyes (Soon and Hameed, 2011). Clays have several advantages: low cost, high surface area, low environmental impact and, in some cases, they contain natural iron that may work as catalyst.

It was suggested that the reaction mechanism in heterogeneous catalysis involve the Fe(III) on the surface of the support and the Fe_2O_3 present on the support:

$$Fe^{3+}\text{-on the surface of Fe\_Clay} + h\nu \rightarrow Fe^{2+}\text{-on the surface of Fe\_Clay} \tag{13.6}$$

$$Fe^{2+}\text{-on the surface of Fe\_Clay} + H_2O_2 \rightarrow Fe^{3+}\text{-on the surface of Fe\_Clay} + HO^{\bullet} + OH^- \tag{13.7}$$

$$\text{Fe-Clay-dye} + HO^{\bullet} \rightarrow \text{reaction intermediates} \rightarrow CO_2 + H_2O \tag{13.8}$$

$$Fe_2O_3 \text{ in Fe-Clay} + \text{dye} + h\nu \rightarrow [\text{dye}^{\bullet} \ldots Fe_2O_3] \text{ in Fe-Clay} \rightarrow \text{dye}^{\bullet+} + Fe_2O_3 \text{ in Fe-Clay} + e^-_{CB} \quad (13.9)$$

$$\text{dye}^{\bullet+} \rightarrow \text{reaction intermediates} \rightarrow CO_2 + H_2O \quad (13.10)$$

Catalytic activity is also originated from a homogeneous process due to iron leaching from the catalyst. Fe^{2+} in solution can be obtained by the photoreduction of $\equiv Fe^{3+}$ under UV radiation. In addition, Fe^{3+} in solution was also produced when $\equiv Fe^{2+}$ is oxidized by H_2O_2. Other transition metal cations can potentially be used as supported catalysts for Fenton or photo-Fenton processes, but only few examples were reported at present (Timofeeva *et al.*, 2009; Yip *et al.*, 2007).

Clays, and specially bentonites, deserve special attention due to their versatility for environmental applications. In several countries as for example Argentina, there are rich natural sources of bentonites that can be used in environmental applications helping the development of the local economies. Montmorillonite is a bentonite with great specific surface area and optimal properties for metal adsorption (Bhattacharyya and Gupta, 2008; Gu *et al.*, 2010; Ijagbemi *et al.*, 2009). In particularly, the uptake of uranium and copper from aqueous solutions by the use of montmorillonites was recently demonstrated (Bhattacharyya and Gupta, 2007; Schlegel *et al.*, 2009). An alternative that was recently investigated has to do with the combination of biomass with clays. Biomass in general and microscopic biomass in particular are very active in the adsorption of metals from solution, allowing concentrating heavy metals from diluted solutions (Shinde *et al.*, 2012; Yipmantin *et al.*, 2011; Volesky, 2007). The hybrid materials produced by combination of both adsorbents seem to be more efficient for the adsorption and removal of metals in solution and to have better coagulation properties. In particular, good results were obtained for the removal of uranium and copper in water using bacterial or fungal biomass respectively (Ohnuki *et al.*, 2005; Olivelli *et al.*, 2013). When raw clays and modified clays are used to remove metals form solution, a new solid waste containing metals is generated, which should be appropriately disposed. As an alternative, if the clays are used to adsorb metals with catalytic activity, they can be used in oxidation processes like Fenton or photo-Fenton.

In this work, we present a comparative study about the use of Fe(III) and Cu(II) supported on montmorillonite as catalyst for the discoloration and mineralization of reactive Orange 16 by photo-Fenton process. Copper containing montmorillonite and bio-montmorillonite obtained after removal of Cu(II) from water were also used to test their performance as catalyst in the same reaction. Reactive Orange 16 was selected as pollutant target due to the requirement of the local industry for technologies to remove dyes from wastewater before its discharge in rivers.

13.2 EXPERIMENTAL SECTION

13.2.1 *Materials*

A bentonite sample (MMT) coming from the Argentine North Patagonia (Río Negro) was used as raw material for all the synthesis described in this work. The MMT mineralogy was evaluated by X-ray diffraction and chemical analysis in previous studies (Iborra *et al.*, 2006; Lombardi *et al.*, 2003) and consists of Na-rich montmorillonite (>99%) with minor phases as quartz and feldspars. Some physicochemical parameters of the raw MMT were determined elsewhere: structural formula $[(Si_{3.89}\ Al_{0.11})(Al_{1.43}Fe^{3+}_{0.28}Mg_{0.30})O_{10}(OH)_2]\ M^+_{0.41}$; cationic exchange capacity (CEC) = 174 meq/100 g clay, isoelectric point (IEP) at pH 2.7 and specific surface area determined by N_2 adsorption (BET method) $S_{N_2} = 34.0\,m^2\,g^{-1}$, and by water adsorption $S_w = 621\,m^2\,g^{-1}$ (Magnoli *et al.*, 2008).

Reactive Orange 16 (RO16 -Sigma) was used as received. Hydrogen peroxide (30%), sulfuric acid and sodium sulfite, all PA quality, from Merck, were also used. Deionized water was obtained with an Osmoion water purifier. The formula of RO16 is given by:

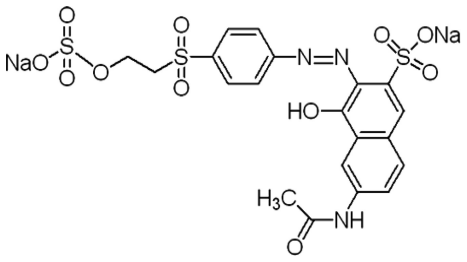

13.2.2 *Iron (III) modified montmorillonite (Fe-MMT)*

Iron chloride hexahydrate (15 g, Aldrich) and montmorillonite (15 g) were respectively dissolved and suspended in acetone (50 mL, Merck). The slurry was stirred for 1 hour, washed with acetone and ethanol, and finally dried at 60°C overnight. The obtained product was named Fe-MMT.

To determine the iron loading, a sample of Fe-MMT was digested in a 5.0 M HCl+HNO_3 acid solution at room temperature. The content of iron in the solution was determined by the thiocyanate method. The iron load was 24 ± 1 mg/g of clay.

13.2.3 *Copper (II) modified montmorillonite (Cu-MMT)*

MMT fired at 500°C for 8 h (3.0 g) was suspended in 100 mL of a 0.050 M $CuSO_4$ (Merck) solution at pH 5.0, and stirred for 1 hour at 50°C. The solid was decanted and washed 3 times with deionized water and dried at 60°C overnight. The obtained material was named Cu-MMT. To determine the copper loading, a sample of Cu-MMT was digested in 1.0 M HNO_3 acid. Cu(II) was determined spectrophotometrically by the dithizone method. The copper loading was 60 ± 2 mg/g of clay.

13.2.4 *Biomodified montmorillonite (Apha-BMMT)*

A copper and uranium resistant acidophilic fungi genus was used, *Aphanocladium* sp. (*Apha* sp.). To generate the clay biopolymer (named as *Apha-BMMT*), the biomass was grown axenically in batch systems with P5 culture medium (1.28 g L^{-1} K_2HPO_4; 3 g L^{-1} $(NH_4)_2SO_4$; 0.25 g L^{-1} $MgSO_4.7H_2O$; 10 g L^{-1} glucose; 0.1 g L^{-1} thiamine; 1% (v/v) microelements solution) containing MMT clay 1% (w/v) and 5% V/V of initial inoculum. Generated Apha-BMMT were recovered by centrifugation (20 minutes, 2200 g, 4°C) and washed with distilled water.

13.2.5 *Adsorption of Cu(II) on MMT and Apha-BMMT*

MMT samples were stabilized by suspension overnight in P5 culture medium, followed by washing with deionized water, centrifugation and drying at 60°C. This material, named *P5-MMT*, was used as sorbent for Cu(II) dissolved in water solutions.

Copper sulfate solutions containing from 0.16 to 7.9 mM copper pH 3.6 were prepared. Duplicate Apha-BMMT or P5-MMT samples (0.1 g) were shaken during 2.25 h (according to previous equilibrium essays, data not shown) in polypropylene tubes with 10 mL aliquots of each solution. After the equilibration time, two samples of 1.0 mL were taken from each tube and centrifuged (5000 g, 8 min). The supernatant was analyzed for copper with the Cuprizone technique, and the solid was reserved for XRD and electrophoretic mobility analysis. The metal adsorbed was calculated as the difference between the initial concentration and that of the supernatant in equilibrium.

The copper adsorption capacity was fitted by Langmuir, Freundlich and sigmoidal isotherms using the SigmaPlot 10.0 software (Statistics – Regression Wizard).

The same procedure was followed to obtain P5-MMT and Apha-BMMT saturated with Cu(II) for testing their catalytic activity in photo-Fenton experiments for the degradation of RO16. The saturated powders were washed several times by centrifugation (until Cu(II) was not detected in the rinsed water) and dried at 60°C. The obtained catalysts were named P5-Cu and Apha-Cu respectively.

13.2.6 *Materials characterization*

Samples of the different materials were characterized by X-ray diffraction (XRD, Siemens D-5000) and by measurements of electrophoretic mobility in KCl 1.0 mM at different pH (EPM, Brookhaven 90-Plus).

13.2.7 *Photo-Fenton experiments*

Photo-Fenton experiments were performed in a batch recirculating system (1.0 L min^{-1} flow rate) consisting of an annular glass reactor (415-mm length, 32-mm internal diameter), a peristaltic pump (APEMA BS6, 50 W), and a thermostatted (25°C) cylindrical reservoir. A blacklight tubular UV lamp (Philips TLD/08, 15 W, 350 nm < λ < 410 nm, maximum emission at 366 nm) was installed inside the annular reactor as the illumination source. Scheme 13.1 shows a flow diagram of the system. The total volume of the circulating mixture was 450 mL, of which 100 mL was inside the photoreactor and constantly irradiated. The catalyst (1 g L^{-1}) was dispersed by continuous stirring in 450 mL of a water solution containing 100 mg L^{-1} of RO16 and the pH adjusted to 3.0 with diluted sulfuric acid. It was experimentally determined that adsorption of RO16 on MMT, Fe-MMT, Cu-MMT, P5-Cu or Apha-Cu was negligible. After 10 min of stabilization under stirring, the pump and the light were turned on, letting the suspension circulate for the reactor for at least 10 min. A 10 mL sample was taken, stabilized with 2 mL of 1.0 M sodium sulfite and stored at 4.0°C. Hydrogen peroxide, 30%, was added to the system in order to obtain the desired H_2O_2 initial concentration. During irradiation, the suspension was vigorously stirred in the reservoir. Samples were taken at certain intervals to determine RO16 and TOC concentrations. The samples were immediately quenched by addition of sodium sulfite in the proportion given above. The solid catalyst was removed from the suspension by centrifuging at 10000 rpm in 2 mL plastic tubes.

RO16 concentration was determined by UV-Vis spectrophotometry with an Ocean optics HR2000 spectrophotometer. Total organic carbon (TOC) was measured with a Shimadzu 5000-A TOC analyzer in the nonpurgeable organic carbon (NPOC) mode. In what follows, we refer to this measurement simply as TOC. Actinometric measurements were performed with ferrioxalate. A photon flow per unit volume ($q^0_{n,p}/V$, where $q^0_{n,p}$ is the incident photon flux and V is the irradiated volume) of 7.4 μ Einstein s^{-1} L^{-1} was calculated for the black-light lamp (assuming 366-nm monochromatic light).

13.3 RESULTS

13.3.1 *Adsorption of Cu(II) on P5-MMT and Apha-BMMT*

Figure 13.1 shows copper adsorption isotherms for P5-MMT and Apha-BMMT.

At low copper concentrations (lower than 2 mM), all the samples show similar adsorption capacity. From 2 mM, the adsorption capacity rises, mainly in the systems with biomass. This sigmoidal shape of isotherms suggested different adsorption sites with different affinities for copper or the existence of a cooperation effect that increases the affinity between copper (II) and adsorption sites. Although the biopolymer had lower adsorption capacity of the biomass or MMT, the coagulation capacity of the system was increased, leading to an improved separation of solids from the solution.

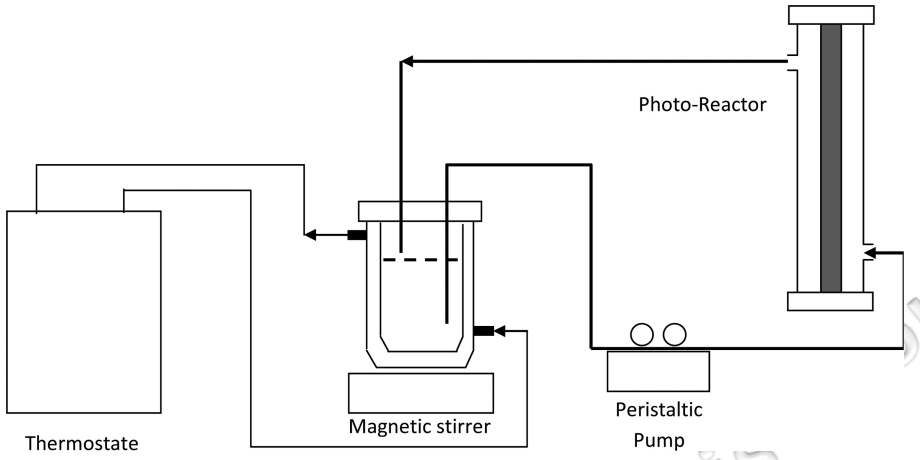

Scheme 13.1. Photo-reactor system flow diagram.

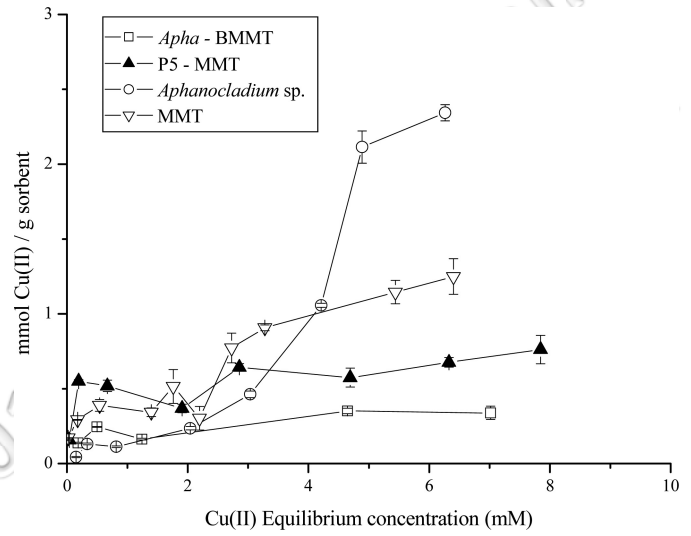

Figure 13.1. Adsorption isotherms of Cu(II) on different substrates.

13.3.2 *Catalysts characterization*

Figure 13.2A shows XRD patterns of the three different solids: MMT, Fe-MMT and Cu-MMT. The d_{001} reflection is the main source to identify the clays (interlayer space). Pure MMT display a diffraction peak at 6.6° that corresponds to a d_{001} basal spacing of 13.6 Å. On the other hand, Fe-MMT shows a diffraction peak at 5.6° that corresponds to a d_{001} basal spacing of 16.5 Å. In the case of Cu-MMT, the reflection peak shifted to 7.6°, which is similar than in the case of MMT fired at 500°C (not shown). The d_{001} basal spacing in these cases is 11.6 Å that indicates the collapse of the structure as consequence of the thermal treatment. The diminution in the intensity of the reflection peak is also due to the disruption of the structure.

The XRD patterns of MMT and BMMT with adsorbed copper was different. A shift of the reflexion peak d_{001} towards smaller values of 2θ was observed for P5-Cu with respect to that found for P5-MMT. The shift of the reflexion peak d_{001}, indicated the entrance of the copper

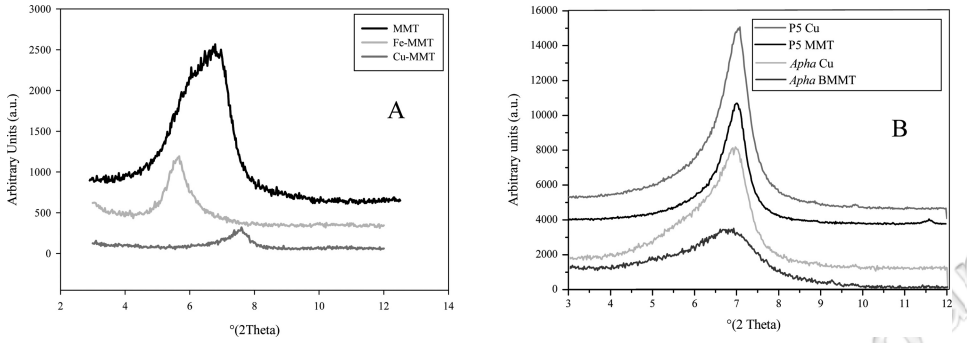

Figure 13.2. XRD Patterns of MMT, Fe-MMT and Cu-MMT (Figure 2A) and P5-MMT, P5-Cu, Apha-MMT and Apha-Cu (Fig. 13.2B).

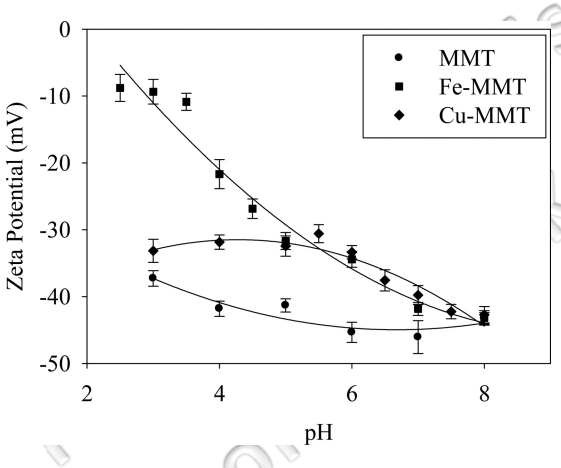

Figure 13.3. Electrophoretic mobility of MMT, Fe-MMT and Cu-MMT at different pH. 0.050 g L^{-1} of the powders were dispersed in 1 mM KCl. pH was adjusted with HNO_3 or KOH as needed.

cation to the clay interlayer. The asymmetrical shape of the reflexion peak d_{001} for all samples with copper indicated the existence of a heterogeneous interlayer. To achieve some precision of the latter behavior, the mathematical decomposition of the reflexion peak d_{001} for P5-Cu and Apha-Cu was performed. Two peaks were found for the d_{001} reflexion peak decomposition of both samples, which confirmed the existence of a heterogeneous interlayer originated by water and copper cations in the interlayer. In Apha-Cu, the input of copper to the interlayer is of lesser extent than in the case of MMT. This decrease may be due to the high affinity of the biomass by Cu(II) that competes with the binding sites into the clay interlayer

Figure 13.3 shows the effect of pH on the electrophoretic mobility of MMT, Fe-MMT and Cu-MMT. MMT electrophoretic mobility is almost independent of pH due to its intrinsic negative charge, which is consequence of its crystalline structure. Proton adsorption on MMT takes place at low pH values, leading to a diminution in the absolute value of ζ-potential. In the case of Fe-MMT, the ζ-potential notably increases as the pH decreases, while Cu-MMT displays a behavior between MMT and Fe-MMT. The effect of Fe(III) on the ζ-potential indicates that iron is present on the surface of the Fe-MMT particles, shifting the isoelectric point to values closer to that corresponding to iron oxides (pH: 7.8–8.5). In the case of Cu(II), there is only a shift of ζ-potential to less negative values, meaning that Cu(II) compensate in part the negative surface charge of MMT.

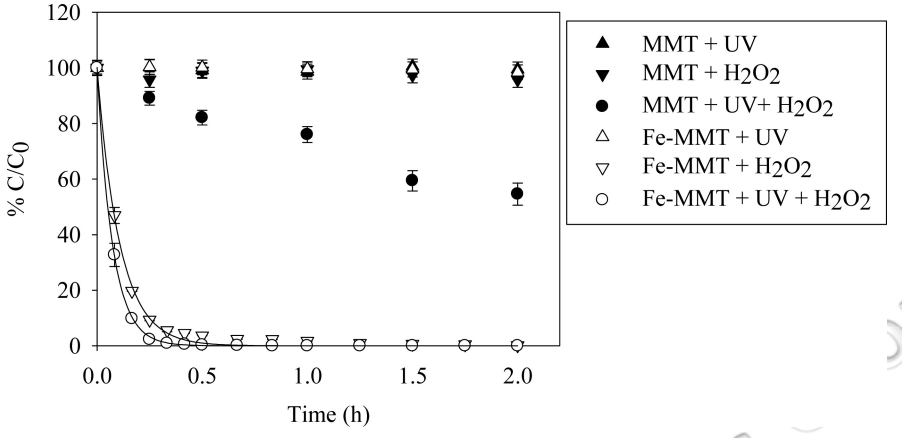

Figure 13.4. Temporal evolution of RO16 in water solutions. RO16 concentration: 100 mg L^{-1}; MMT, Fe-MMT concentration: 1.0 g L^{-1}; pH = 3.0; $[H_2O_2]_0 = 100$ mM.

Table 13.1. Pseudo first order constant rate and correlation coefficients corresponding to the experiments shown in Figure 13.3.

System	k_1 (s^{-1})	r^2
MMT + UVA + 0.1 M H_2O_2pH 3	0.36 ± 0.01	0.9891
Fe-MMT + 0.1M H_2O_2 pH 3	9.2 ± 0.3	0.9968
Fe-MMT + UVA + 0.1 M H_2O_2 pH 3	13.7 ± 0.2	0.9998
Fe-MMT + 0.05 M H_2O_2 pH 3	10.3 ± 0.7	0.9936
Fe-MMT + UVA + 0.05 M H_2O_2 pH 3	18.2 ± 0.6	0.9991

13.3.3 *Photo-Fenton experiments*

Figure 13.4 shows the temporal evolution of the concentration of RO16 in water solutions exposed to different treatments that use Fe-MMT as catalyst, together with different controls.

Degradation of the dye in the presence of MMT + UV, MMT + H_2O_2 or Fe-MMT+UV was negligible. However, when Fe-MMT was used in the presence of H_2O_2 or H_2O_2 + UVA, the degradation of the dye was very fast due to the occurrence of Fenton and photo-Fenton processes, respectively. It is noticeably that photo-Fenton is slightly more efficient than Fenton. The dye was also discolored in the presence of H_2O_2 and UVA with or without MMT (only the data obtained in the presence of MMT are shown in Fig. 13.4), but with a much lower degradation rate.

The degradation rate could be described by a first order kinetics; the pseudo first order constants are given in Table 13.1. It is notable the increment in k_1 when the Fenton experiments were run under UVA irradiation.

Table 13.1 also shows the effect of H_2O_2 concentration on the pseudo first order constant. When the concentration decreased from 0.100 M to 0.05 M, the constant rates slightly increased.

Figure 13.5 shows the temporal evolution of RO16 water solutions exposed to different oxidation treatments using Cu-MMT. The degradation rate was noticeably lower than in the experiments run with Fe-MMT. The Fenton-like reaction with Cu-MMT was even slower than with pure MMT. However, under UVA illumination, the degradation rate increased and the solutions were completely bleached in 5 hours.

The color of the solution during degradation shifted to red when Cu-MMT was used as catalyst. This effect was observed with naked eye and suggests that the mechanism of degradation is different depending if Fe-MMT or Cu-MMt is used as catalyst in photo-Fenton process. Figure

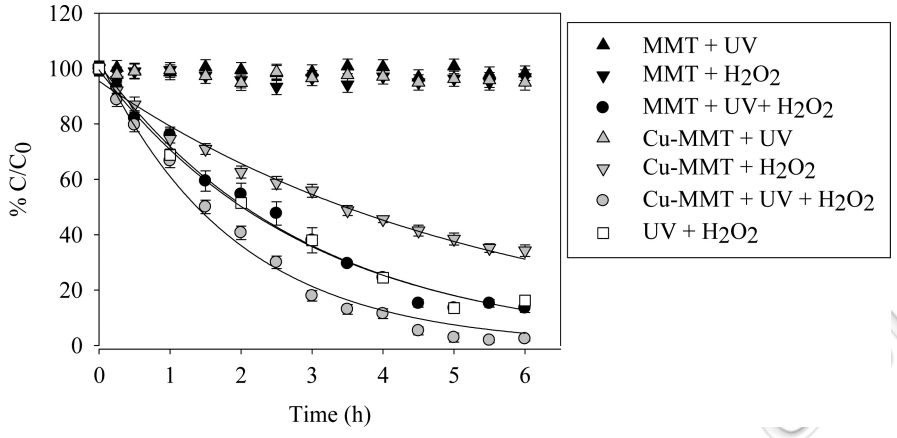

Figure 13.5. Temporal evolution of RO16 in water solutions. RO16 concentration: 100 mg L^{-1}; MMT, Cu-MMT concentration: 1.0 g L^{-1}, pH = 3.0; $[H_2O_2]_0$ = 100 mM.

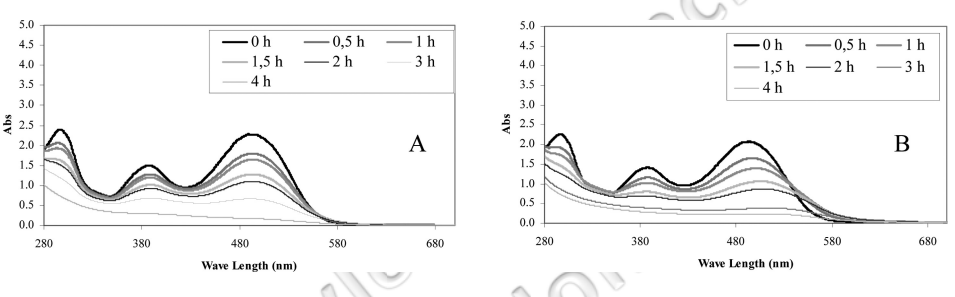

Figure 13.6. UV-vis spectra of samples taken during photo-Fenton degradation 100 mg L^{-1} RO16, pH 3.0, catalyst concentration 1.0 g L^{-1}, $[H_2O_2]$ = 100 mM. (A) MMT, (B) Cu-MMT. Part of the copper was released to the solution at pH 3.0; its concentration after 24 h of irradiation was 18 ± 2 mg L^{-1}.

13.6 shows UV-vis spectra of solutions taken at different times during the degradation by photo-Fenton of RO16, using MMT (Fig. 13.6A) or Cu-MMT (Fig. 13.6B). In the first case, the intensity of the band centered at 490 nm decreased with treatment time without changes in the maximum position. In the second case, the position of the maximum shifted to higher wavelength (red) as the intensity of the band decreased.

The diminution of the total organic carbon content (TOC) during the treatment is another important consequence of the oxidation treatment. Figure 13.7 shows the temporal evolution of TOC during a wide period of time. Fenton and photo-Fenton with Fe-MMT quickly reduced TOC until approximately 65 or 57% of TOC remained in solution, respectively. Photo-Fenton process was faster than Fenton and led to lower TOC at the end of the process. On the other hand, Cu-MMT worked slowly at the beginning but led to lower TOC at the end of the process. These results also show that the mechanism involved in the degradation of the dye in the presence of Fe-MMT or Cu-MMT was different. Pure MMT also shows activity in the reduction of TOC in solution, but the reduction rate was lower and a higher percentage of TOC remained at the end of the experiment.

Degradation of RO16 was also performed in the presence of other copper containing catalysts as P5Cu (Cu(II) adsorbed on MMT) and Apha Cu (Cu(II) adsorbed on BMMT), to compare the activity of these materials (obtained as "waste" in the adsorption of Cu(II) from aqueous solutions) with Cu-MMT, especially prepared as photo-Fenton type catalyst. Figures 13.8A and B show discoloration rate and TOC evolution, respectively.

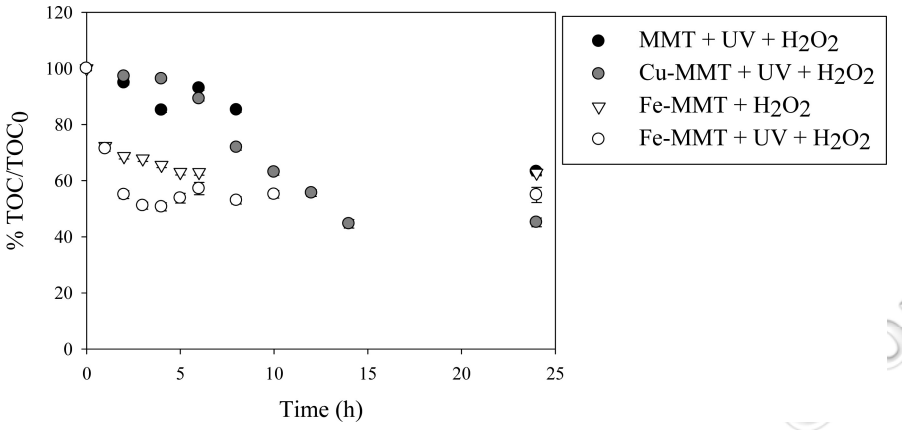

Figure 13.7. TOC evolution during Fenton and photo-Fenton process using different catalysts. In all the experiments, $[H_2O_2]_0 = 0.100\,M$, catalyst concentration: $1.0\,g\,L^{-1}$, RO16 concentration: $100\,mg\,L^{-1}$, pH = 3.0.

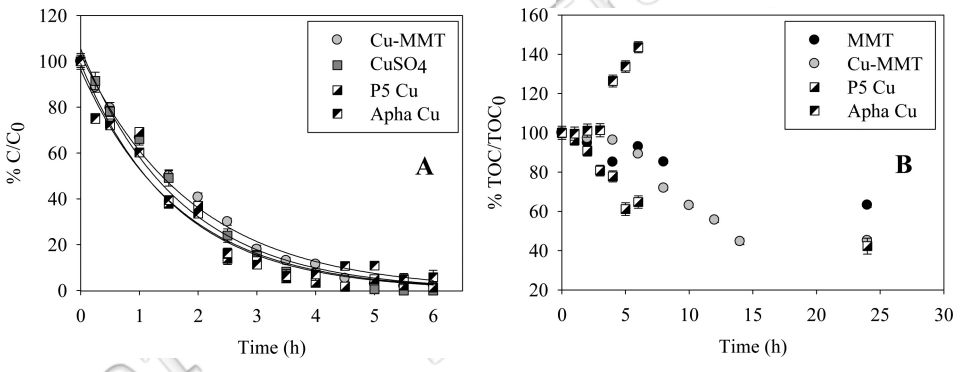

Figure 13.8. Evolution of color (A) and TOC (B) during photo-Fenton process using different catalyst containing Cu(II). In all the experiments $[H_2O_2]_0 = 0.100\,M$, catalyst concentration: $1.0\,g\,L^{-1}$, RO16 concentration: $100\,mg\,L^{-1}$, pH = 3.0.

All the Cu(II)-containing catalysts displayed similar behavior with respect to their activity in discoloration. The kinetics could be described by a pseudo-first order law (the parameters are given in Table 13.2). An experiment was done as a control for homogeneous catalysis using $CuSO_4$ as a source of Cu(II) (see Fig. 13.8A). The concentration of Cu(II) in solution ($20.0\,mg\,L^{-1}$) was close to that obtained by leaching from Cu-MMT after 24 h of reaction at pH 3.0 ($18\,mg\,L^{-1}$). The behavior of this control experiment was similar to those in the experiments with supported Cu(II), indicating that most of the catalytic activity may be due to dissolved Cu(II).

Figure 13.8B shows that the evolution of TOC was similar for the systems with Cu-MMT and P5-Cu, the system with P5-Cu being slightly faster. At the end of the experiments, the content of TOC was similar in both cases and lower than that corresponding to pure MMT. In the period 15–24 h, TOC did not decrease in spite that there was H_2O_2 in solution (after 14 h of treatment, 80% of the initial H_2O_2 remained in all copper systems, measured by the VO^{3-} method (Pupo Nogueira *et al.*, 2005). The situation was completely different for Apha-Cu, where TOC remained constant during the first 5 h of treatment, but rapidly increased at longer times.

Table 13.2. Pseudo first order constant rate and correlation coefficients corresponding to the experiments shown in Figs. 13.5 and 13.8A.

System	k_1 (s^{-1})	r^2
MMT + UVA + 0.1 M H_2O_2 pH 3	0.36 ± 0.01	0.9891
Cu-MMT + 0.1 M H_2O_2 pH 3	0.19 ± 0.01	0.9886
Cu-MMT + UVA + 0.1 M H_2O_2 pH 3	0.53 ± 0.02	0.9895
20 mg L^{-1} $CuSO_4$ + UVA + 0.1 M H_2O_2, pH 3	0.59 ± 0.04	0.9829
P5-Cu + UVA + 0.1 M H_2O_2 pH 3	0.62 ± 0.06	0.9638
Apha Cu + UVA + 0.1 M H_2O_2 pH 3	0.60 ± 0.04	0.9771

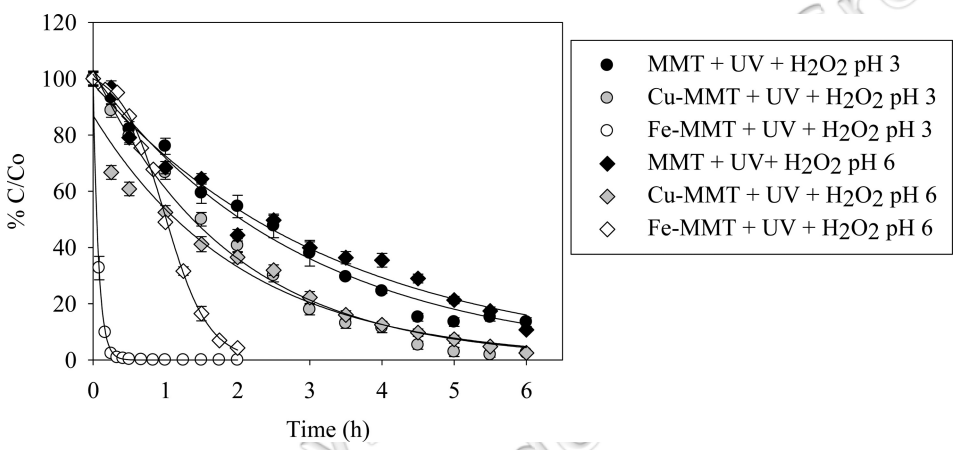

Figure 13.9. Temporal evolution of RO16 during photo-Fenton like treatment at pH 3.0 or 6.0. RO16 concentration: 100 mg L^{-1}; catalyst concentration: 1.0 g L^{-1}, $[H_2O_2]_0 = 100$ mM.

It is well established that pH has a notable effect on the catalytic activity in Fenton and photo-Fenton processes. Figure 13.9 shows the evolution of RO16 concentration using both catalysts at two different initial pH values: 3.0 or 6.0[1]. In this Figure, the difference in degradation rate when Fe-MMT or Cu-MMT was used as catalyst is remarked; as shown in Tables 13.1 and 13.2, all systems except Fe-MMT at pH 6.0 can be modeled by a pseudo first order kinetics, being the constant rate more than one order higher for the Fe-MMT systems than for the Cu-MMT systems. The effect of pH on the discoloration rate when Fe-MMT was used as catalyst was notable. At pH 6.0, there was an induction period that delays the discoloration of the solution, but after the first 40 minutes, discoloration occurred relatively fast. In the case of Cu-MMT, at pH 6.0 the discoloration was faster at the beginning of the treatment than at pH 3.0. As the treatment went further, the reaction slowed down and, at the end of the treatment, both systems reached approximately the same degree of discoloration. It is very interesting that when pure MMT was used as catalyst, the discoloration rate was quite similar at both pH values. It should be mentioned that in the experiments made at initial pH 6.0, the pH decreased during the experiment, being 4.5 the final value in all cases.

Figure 13.10 shows the evolution of TOC in the experiments performed at different pH values. In the case of Fe-MMT, TOC diminution followed a pattern similar to discoloration at each pH. At pH 6.0, TOC diminutions started after an induction period but, at the end of the experiment,

[1]The absorption spectrum of RO16 is independent of pH in the range 2–8.

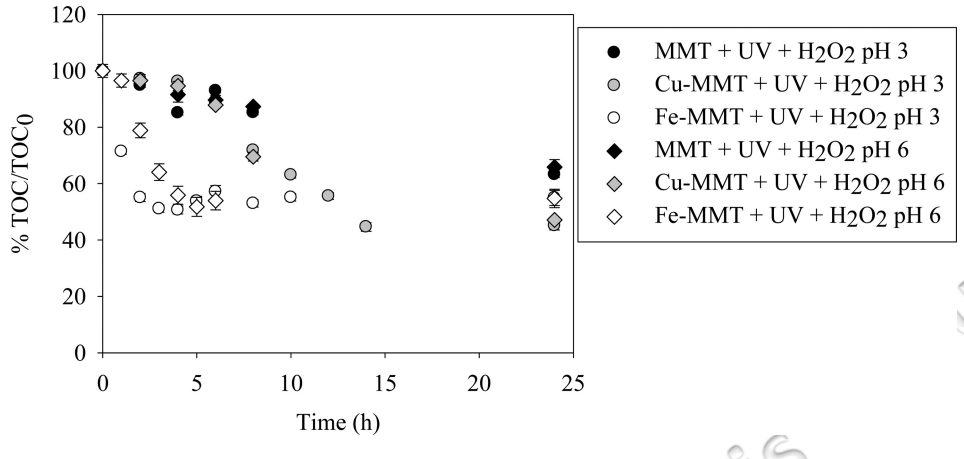

Figure 13.10. TOC evolution during photo-Fenton like treatment at pH 3.0 or 6.0. RO16 concentration: 100 mg L^{-1}; catalyst concentration: 1.0 g L^{-1}, $[H_2O_2]_0 = 100$ mM.

TOC values were similar for both pH values. In the case of pure MMT and Cu-MMT, similar behavior was observed at pH 3.0 and 6.0. The more remarkable result of this experiment is that for the different catalysts the final TOC value was similar at both pH values.

13.4 DISCUSSION

The incorporation of metal cations into MMT can be done by different ways. Cation exchange of the exchangeable cations of the clay may be the simplest way, although the content of metal cation could be too low. Impregnation and pillaring appears as more effective methods. Also, the metals can be simply adsorbed at the surface. Incorporation of metals into the inter-lamellar spaces of the clays produced an increment in the d_{001} basal spacing that could be detected by XRD analysis. Figure 13.1 shows clearly that Fe-MMT presented a d_{001} spacing larger than pure MMT (16.5 and 13.6 Å, respectively), which indicates that Fe(III) was incorporated into the MMT structure. On the other hand, Cu-MMT was prepared by impregnation of calcined MMT. In this case, the XRD analysis indicated that the basal spacing was smaller than in raw MMT (11.6 Å), meaning the partial collapse of the structure (which is supported by the diminution in peak intensity). Consequently, Cu(II) was not introduced between layers and was mostly presented at the surface of the particles. In the case of P5-Cu, the d_{001} basal spacing increased indicating that some Cu(II) was exchanged into MMT. It should be noted that the radii of Cu^{2+} and $Cu(H_2O)_6^{2+}$ (octahedral) are 0.94 Å and 1.96 Å respectively (Persson, 2010), so there is plenty of room for Cu(II) in the interlayer space of MMT. In all the cases, the metals were also adsorbed at the surface as can be deduced from the changes in electrophoretic mobility shown in Figure 13.2. The adsorption of metallic cations decreased the surface charge of MMT, decreasing the mobility and shifting the isoelectric point to lower pH values. Metals at MMT surface showed catalytic activity in both Fenton and photo-Fenton reactions. The sigmoidal shape displayed by the adsorption isotherm of Cu(II) on BMMT could be due to the heterogeneity of sites available on this adsorbent. Besides the interlayer spaces and the surface sites typically present in clays, BMMT also display functional groups present in the biomass attached to the MMT. These groups provide a larger quantity of metal binding sites and greater affinity to the system. Evidence of adsorption of copper in interlayer space is shown by XRD analysis (Fig. 13.2B). Studies of Cu(II) interactions with fungi and bacteria showed that Cu(II) may be associated with the functional groups on the cellular

surface. FT-IR analysis indicates that copper is bound to sites in the interlayer of MMT and amines, amides and carboxylates of proteins and carbohydrates of biomass (data not shown).

RO16 was quickly degraded by both Fenton and photo-Fenton process catalyzed by Fe-MMT. The dye was also partially degraded by the simultaneous presence of MMT, H_2O_2 and UVA; this effect may be a consequence of sensitization of the dye by UVA absorption (see Fig. 13.6A), or due to the leaching of a small amount of iron from the MMT that could trigger some photo-Fenton activity. It should be noted that natural MMT has iron in its composition that can be leached to the solution at pH 3 (0.03 mM measured by atomic absorption spectroscopy). Photo-Fenton was a little more active than Fenton, as can be observed by comparing the values of the pseudo-first order constants shown in Table 13.1. The degradation rate of RO16 by photo-Fenton increased when the concentration of H_2O_2 was reduced to 0.050 M. This effect may be a consequence of the well-known scavenger effect of H_2O_2 on $HO^\bullet$ radicals represented by reactions (13.11) and (13.12) (Pupo Nogueira *et al.*, 2007):

$$HO^\bullet + H_2O_2 \rightarrow HO_2^\bullet + H_2O \tag{13.11}$$

Hydroperoxyl radicals display a much lower redox potential (1.42 V *vs.* NHE) than $HO^\bullet$ radicals (2.73 V *vs.* NHE), and can be eliminated by Fe^{3+} in solution:

$$Fe^{3+} + HO_2 \rightarrow Fe^{2+} + O_2 + H^+ \tag{13.12}$$

The excess of H_2O_2 very likely reduced the concentration of $HO^\bullet$ available for RO16 oxidation, diminishing the degradation rate as the H_2O_2 concentration increased. The stoichiometric ratio dye:H_2O_2 for oxidation of RO16 is 1:40. In this study, the ratio was 10 and 20 times higher in favor to H_2O_2 to allow a comparison between the experiments performed with the catalysts containing Cu(II) or Fe(III).

When Cu-MMT was used as catalyst, discoloration of RO16 was observed in the dark and under illumination, but the degradation rate was notably lower than in the case of Fe-MMT. In the dark, the discoloration was even slower than with pure MMT. UVA illumination produced a marked increment in discoloration rate; the difference in the degradation rate observed in the dark with respect to UVA illumination was higher than in the case of Fe-MMT (compare Figs. 13.3 and 13.4). The activity of Cu(II) in Fenton and photo-Fenton processes was documented before, although the details are less known than in the case of Fe(II)/Fe(III) (Ciesla *et al.*, 2004; Ghiselli *et al.*, 2004; Masarwa *et al*., 1988; Sykora, 1997). Cu(II) has to be reduced to Cu(I) to enter the typical Fenton cycle that produce $HO^\bullet$ and regenerates the catalyst:

$$Cu^{2+} + 1\,e^- \rightarrow Cu^+ \tag{13.13}$$

$$Cu^+ + H_2O_2 \rightarrow Cu^{2+} + OH^- + HO^\bullet \tag{13.14}$$

The reduction of Cu(II) to Cu(I) may be mediated by reaction with organic compounds or by reduction with HO_2^- or $O_2^{\bullet -}$ (Ciesla *et al.*, 2004; Sykora, 1997):

$$Cu^{2+} + HO_2^- \rightarrow Cu^+ + O_2^- + H^+ \tag{13.15}$$

$$Cu^{2+} + O_2^- \rightarrow Cu^+ + O_2 \tag{13.16}$$

It was proposed before that because copper often disproportionate H_2O_2 intermediates, converting them to H_2O, aqueous Cu(II) may reduce the oxidative capacity of H_2O_2 (Ghiselli *et al.*, 2004). This effect may explain the low activity of Cu-MMT in Fenton reaction (even lower than that of MMT + H_2O_2 + UVA).

It was determined that copper can be involved in photoredox cycles that can explain their activity in photo-Fenton processes. Copper complexes can be excited by sunlight when the ionization energy of the ligands coordinated to Cu(II) is not too high. As consequence of the reactive decay of the excited state by inner sphere electron transfer, the Cu(II) central atom is reduced to Cu(I), whereas a ligand is oxidized to its radical and leaves the coordination sphere (Ciesla *et al.*, 2004):

$$[Cu^{II}L_x]^{2+} \xrightarrow{h\nu} [Cu^{I}L_{x-1}]^+ + L^+ \tag{13.17}$$

Photoproduced Cu(I) can be oxidized to Cu(II) by O_2 or by H_2O_2:

$$Cu^+ + O_2 \rightarrow Cu^{2+} + O_2^{\bullet -} \tag{13.18}$$

$$Cu^+ + H_2O_2 \rightarrow Cu^{2+} + HO^{\bullet} + OH^- \tag{13.19}$$

The oxidized ligands can be involved in redox process that lead to the oxidation of the same ligands or other organics present in the solution.

As shown in Figure 13.5, the discoloration process of RO16 in the presence of UVA light was preceded by the formation of a red intermediate. That means that the mechanism of degradation involves a first step of oxidation but preserving the aromatic and conjugated structure. The reaction may involve the formation of a coordination complex between Cu(II) and the dye, which is further photooxidized, starting the redox cycle. As shown in Figure 13.5, the dye and its colored byproducts have absorption bands in the UVA range, which can explain its photoactivity. Studies involving $HO^{\bullet}$ scavengers to identify the effect of hydroxyl radicals in the oxidation process and isolation of the red byproduct for chemical characterization are in course to check the previous hypothesis. At this point, it is not clear if at pH 3.0 the Cu(II) involved in the process is the aqueous copper or the immobilized copper. As it was explained in the Results section, similar results were obtained when Cu-MMT was replaced by Cu(II) in a concentration equivalent to that obtained after Cu-MMT leaching. However, as will be discussed later, at pH 6.0, Cu(II) was not leached to the solution but photo-Fenton activity was also observed.

In the literature, there are few reports about supported copper as Fenton or photo-Fenton catalyst. Recently, Yip *et al*. (2007) reported the photocatalytic activity of clay supported copper in photo-Fenton processes, but the catalyst was prepared by chemical vapor deposition and reduced to Cu(I); also the light source was UVC. In spite of the differences in the preparation of the catalyst, there were several similarities with the results reported here; for example, TOC could be successfully reduced during the treatment. By comparing the results of both works, it seems that reduction of Cu(II) to Cu(I) produces a more active catalyst for photo-Fenton process, but a reduction step is necessary and UVC is needed as light source.

Discoloration itself is an important result because it reduces the visual impact of the pollutants and diminish the absorption of the incident light, which is necessary for the growing of biota that may contribute to further elimination of byproducts. However, the total organic content is also an important issue because it is related to the presence of recalcitrant pollutants that may be more toxic than the dye itself (as was discussed in the introduction). The spectra shown in Figure 13.6 indicate the elimination of aromatic rings during the degradation of RO16, as can be deduced from the diminution of the intensity of the absorption bands centered at 385 and 290 nm. This result explains the fast discoloration of the solution exposed to the Fenton treatment. On the other hand, the analysis of the evolution of TOC content during the degradation experiments showed that at the beginning of the reaction TOC decreased with a similar trend than discoloration, but mineralization stopped after TOC reached 40–60% of its initial value. Similar results were recently reported in the degradation of other naphthalene azo dyes by the Fenton reaction (Zhu *et al.*, 2012). Degradation of azo dyes usually involves the elimination of the azo bound as N_2, followed by different steps that include OH incorporation to the aromatic ring, dealkylation and ring opening. As it is documented in the literature, the hydroxylation of benzene and naphthalene rings leads to ring opening, giving short-chain carboxylic acids (Stylidi *et al.*, 2003). The low TOC degradation is usually assigned to the generation of alkyl carboxylic acids with relatively low molecular weight (Klamerth *et al.*, 2009; Zhu *et al*., 2012). Such compounds, as acetic, oxalic or maleic acid, are recalcitrant with respect to Fenton or photo-Fenton treatments. In the presence of UVA, light TOC elimination was faster, as can be seen in Figure 13.7. This effect is related with the generation of $HO^{\bullet}$ by photoreaction of $Fe(OH)_2^+$. As the reaction advanced, recalcitrant byproducts formed and TOC remained stable, but at lower percentage than in the dark experiments.

In the case of the copper containing catalysts Cu-MMT and P5-Cu, the initial rate of TOC diminution in the photo-Fenton reaction was notably lower than the corresponding to Fe-MMT. However, TOC decreased continuously during the first 15 h of treatment, reaching at the end of the experiment lower TOC than in the Fe-MMT case. P5-Cu resulted more active than Cu-MMT in the elimination of TOC, probably due to the higher area of this material that was not exposed to thermal treatment. The reduction of TOC and the discoloration of RO16 observed with P5-Cu indicate that this material, obtained by adsorption of copper in water, can be used as catalyst for the elimination of organic pollutants in water. Some improvements are needed in order to reduce the secondary contamination produced by the release of copper to the solution at pH 3.0. In the case of Apha-Cu, TOC increased after the first five hours of treatment due to the elimination of the original biomass attached to MMT.

pH had an important role in the degradation of RO16 by photo-Fenton process under the condition studied in this work, as it is shown in Figure 13.9. Because the studied pH values had no effect on the degradation of the dye in the absence of catalyst (similar discoloration performance was observed in experiments with MMT, H_2O_2 and UVA), the changes in the discoloration rate at pH 3.0 or 6.0 can be related with changes in the activity of the catalysts or in the reaction mechanisms. It is well known that when iron species are used as catalyst, pH has an important effect on the efficiency of homogeneous Fenton and photo-Fenton processes. The optimal pH is close to 3. Lower pH produces less active iron species in solution (as $Fe(H_2O)_6^{3+}$) and decreases the production of $HO^{\bullet}$ from H_2O_2 (the specie $H_3O_2^+$ is more reluctant to the production of radicals); in addition, $HO^{\bullet}$ are scavenged by H^+ (Herney-Ramirez *et al.*, 2010). Higher pH leads to precipitation of FeOOH, removing iron from solution, with a consequent diminution in the degradation rate. In iron based heterogeneous Fenton and photo-Fenton, the effect of pH follows the same trend as in the homogeneous process, but the effects are not as dramatic due to the immobilization of the active species. As shown in Figure 13.9, RO16 was discolored at both studied pH values. Because iron is supported, the change in speciation seems to be less affected by pH. The immobilized Fe(III) species cannot be easily transformed in $Fe(H_2O)_6^{3+}$ at low pH or $Fe(OH)_3$ at high pH. Also, due to the interaction of Fe(III) with the clay sheets, the speciation is different and less sensitive to pH changes (De Leon *et al.*, 2008; Najjar *et al.*, 2007). Figure 13.9 also shows that at pH 6.0 Fe-MMT present an induction time before discoloration take place. At present, the origins of this phenomenon are unknown but may be related with the decrease in the pH that took place during the performance of the process (the final pH was 4.5), as reported by Zhang *et al.* (2011). Lower pH leads to the release of small amounts of iron to the solution, which may enhance the degradation rate. The time necessary to reduce the pH and leach iron may explain the induction time.

Although discoloration rate and TOC removal started with a lower rate at pH 6.0 with respect to 3.0, the dye was removed with an acceptable rate and the percentage of mineralization was the same at both pH values (see Fig. 13.10). Because working at pH 6.0 is safer, demand less preparation of the wastewater (which in the case of textiles is usually at pH over 7) and no special acid resistant equipment is needed, it is worth to work at pH 6 in spite of some reduction in degradation rate.

In the case of Cu-MMT, similar discoloration rate and TOC diminution rate were observed at both studied pH values, but a small increment in the initial discoloration rate was observed at pH 6.0 and Cu(II) was not leached to the solution. Although there are relatively few antecedents in the use of Cu(II) as catalyst, the stability of its performance with pH was reported before (Yip *et al.*, 2007). The reasons of this behavior are not clear but may be related with the hydrolytic performance of Cu(II) in water. These results are very promissory for the future application of copper based catalyst in photo-Fenton like processes, because the degree of mineralization is usually higher than that for the iron based catalyst, they are less pH dependent and, at pH 6.0, Cu(II) leaching is very low. Besides, the adsorbents used for copper removal, and other copper enriched wastes (Huanosta-Gutierrez *et al.*, 2012) can be used as catalysts in Fenton like processes.

13.5 CONCLUSIONS

Montmorillonite (MMT) and their iron and copper modifications result attractive materials for water decontamination. The adsorptive capacity of MMT is appropriate for removal of heavy metals from water. Fe-MMT is very active as catalyst for the discoloration of dyes in water by Fenton or photo-Fenton like process at initial pH 3.0 and 6.0. TOC diminution reaches approximately 40% of the initial value due to the production of recalcitrant intermediates. Cu-MMT is also active as catalyst at initial pH 3.0 and 6.0, but only in photo-Fenton like processes. The discoloration rate is lower than that corresponding to Fe-MMT, but the degree of mineralization is higher, reaching values close to 60% of the initial TOC. The mechanism involved in the oxidation is different than the corresponding to Fe-MMT, leading to the production of other dyes before discoloration. Leaching of Cu(II) may be a problem at pH 3.0 but not at pH 6.0, while the activity is quite similar. The waste material obtained after removing Cu(II) from water was successfully used as catalyst in photo-Fenton like processes.

ACKNOWLEDGEMENTS

This work was performed as part of FONARSEC program, FSNano 2010.

REFERENCES

Anipsitakis, G. & Dionysiou, D.: Transition metal/UV-based advanced oxidation technologies for water decontamination. *Appl. Catal.* B 54 (2004), pp. 155–163.

Asgher, M.: Biosorption of reactive dyes: A review. *Water Air Soil Pollut*. 223 (2012), pp. 2417–2435.

Bautista, P.; Mohedano, A.F.; Gilarranz, M.A.; Casas, J.A. & Rodriguez, J.J.: Application of Fenton oxidation to cosmetic wastewaters treatment. *J. Hazard. Mater.* 143 (2007), pp. 128–134.

Bayo, J.: Kinetic studies for Cd(II) biosorption from treated urban effluents by native grapefruit biomass (*Citrus paradisi* L.): The competitive effect of Pb(II), Cu(II) and Ni(II). *Chem. Eng. J.* 191 (2012), pp. 278–287.

Bhattacharyya, K.G. & Gupta, S.S.: Adsorptive accumulation of Cd(II), Co(II), Cu(II), Pb(II), and Ni(II) from water on montmorillonite: Influence of acid activation. *J. Colloid Interface Sci.* 310 (2007), pp. 411–424.

Bhattacharyya, K.G. & Gupta, S.S.: Adsorption of a few heavy metals on natural and modified kaolinite and montmorillonite: A review. *Adv. Colloid Interface Sci.* 140 (2008), pp. 114–131.

Ciesla, P., Kocot, P., Mytych, P. & Stasicka, Z.: Homogeneous photocatalysis by transition metal complexes in the environment. *J. Molec. Catal.* A: *Chem.* 224 (2004), pp. 17–33.

Dhaouadi, A. & Adhoum, N.: Heterogeneous catalytic wet peroxide oxidation of paraquat in the presence of modified activated carbon. *Appl. Catal.* B: *Environ.* 97 (2010), pp. 227–235.

De Leon, M.A., Castiglioni, J., Bussi, J. & Sergio, M.: Catalytic activity of an iron-pillared montmorillonitic clay mineral in heterogeneous photo-Fenton process. *Catal. Today* 133 (2008), pp. 600–608.

Ghiselli, G.F., Jardim, W., Litter, M.I. & Mansilla, H.D.: Destruction of EDTA using Fenton and photo-Fenton-like reactions under UV-A irradiation. *J. Photochem. Photobiol.* A: *Chem.* 167 (2004), pp. 59–67.

Gu, X., Evans, L.J. & Barabash, S.J.: Modeling the adsorption of Cd (II), Cu(II), Ni (II), Pb (II) and Zn (II) onto montmorillonite. *Geochim. Cosmochim. Acta* 74 (2010), pp. 5718–5728.

Hazrat A.: Biodegradation of synthetic dyes—A review. *Water Air Soil Pollut.* 213 (2010), pp. 251–273.

Herney-Ramirez, J., Vicente, M.A. & Madeira, L.M.: Heterogeneous photo-Fenton oxidation with pillared clay-based catalysts for wastewater treatment: A review. *Appl. Catal.* B: *Environ.* 98 (2010), pp. 10–26.

Hosseini Koupaie, E., Alavi Moghaddam, M.R. & Hashemi, S.H.: Evaluation of integrated anaerobic/aerobic fixed-bed sequencing batch biofilm reactor for decolorization and biodegradation of azo dye Acid Red 18: Comparison of using two types of packing media. *Biores. Technol.* 127 (2013), pp. 415–421.

Huanosta-Gutiérrez, T., Dantas, R. F., Ramírez-Zamora, R.M. & Esplugas, S.: Evaluation of copper slag to catalyze advanced oxidation processes for the removal of phenol in water. *J. Hazard. Mater.* 213–214 (2012), pp. 325– 330.

Idel-aouad, R., Valiente, M.; Yaacoubi, A., Tanouti, B. & López-Mesas, M.: Rapid decolourization and mineralization of the azo dye C.I. Acid Red 14 by heterogeneous Fenton reaction. *J. Hazard. Mater.* 186 (2011), pp. 745–750.

Ijagbemi, C.O., Baek, M.H. & Kim, D.S.: Montmorillonite surface properties and sorption characteristics for heavy metal removal from aqueous solutions. *J. Hazard. Mater.* 166 (2009), pp. 538–546.

Khan, R., Bhawana P. & Fulekar, M.H.: Microbial decolorization and degradation of synthetic dyes: A review. *Rev. Environ. Sci. Biotechnol.* 12:1 (2013), pp. 75–97.

Klamerth, N., Gernjak, W., Malato, S., Aguera, A. & Lendl, B.: Photo-Fenton decomposition of chlorfenvinphos: Determination of reaction pathway. *Water Res.* 43 (2009), pp. 441–449.

Lee, Y. & Lee, W.: Degradation of trichloroethylene by Fe(II) chelated with cross-linked chitosan in a modified Fenton reaction. *J. Hazard. Mater.* 178 (2010), pp. 187–193.

Lofrano, G., Meriç, S.V., Belgiorno, N.A. & Napoli, R.M.A.: Fenton and photo-Fenton treatment of a synthetic tannin used in leather tannery: A multi approach study. *Water Sci. Technol.* 55 (2007), pp. 53–61.

Magnoli, A.P., Tallone, L., Rosa, C.A.R., Dalcero, A.M., Chiacchiera, S.M. & Torres Sanchez, R.M.: Commercial bentonites as detoxifier of broiler feed contaminated with aflatoxin. *Appl. Clay Sci.* 40 (2008), pp. 63–71.

Masarwa, M., Cohen, H., Meyerstein, D., Hickman, D.L., Bakac, A. & Espenson, J.H.: Reactions of low-valent transition-metal complexes with hydrogen peroxide. Are they "Fenton-like" or not? The case of Cu^{+} and Cr^{2+}aq. *J. Am. Chem. Soc.* 110 (1988), pp. 4293–4297.

Meriç, S., Lofrano, G. & Belgiorno, V.: Treatment of reactive dyes and textile finishing wastewater using Fenton's oxidation for reuse. *Int. J. Environ. Pollut.* 23 (2005), pp. 248–258.

Montes, S., Montes-Atenas, G., Salomo, F., Valero, E. & Diaz, O.: On the adsorption mechanisms of copper ions over modified biomass. *Bull. Environ. Contam. Toxicol.* 76 (2006), pp. 171–178.

Najjar, W., Azabou, S., Sayadi, S. & Ghorbel, A.: Catalytic wet peroxide photo-oxidation of phenolic olive oil mill wastewater contaminants: Part I. Reactivity of tyrosol over (Al–Fe)PILC. *Appl. Catal.* B: *Environ.* 74 (2007), pp. 11–18.

Neamtu, M., Yediler, A., Siminiceanu, I. & Kettrup, A.: Oxidation of commercial reactive azo dye aqueous solutions by the photo-Fenton and Fenton-like processes. *J. Photochem. Photobiol.* 161 (2003), pp. 87–93.

Ohnuki, T., Yoshida, T., Ozaki, T., Samadfam, M., Kozai, N., Yubuta, K., Mitsugashira, T., Kasama, T. & Francis, A.J.: Interactions of uranium with bacteria and kaolinite clay. *Chem. Geol.* 220 (2005), pp. 237–243.

Olivelli, M., Curutchet G. & Torres Sánchez R.: Uranium uptake by montmorillonite-biomass complexes. *Ind. Eng. Chem. Res.* 52:6 (2013), pp. 2273–2279.

O'Neill, C., Hawkes, F.R., Hawkes, D.L., Lourenco, N.D., Pinheiro, H.M. & Delee, W.: Color in textile effluents sources, measurement, discharge consents and simulation: A review. *J. Chem. Technol. Biotechnol.* 74 (1999), pp. 1009–1018.

Persson, I.: Hydrated metal ions in aqueous solution: How regular are their structures? *Pure Appl. Chem.* 82 (2010), pp. 1901–1917.

Pignatello, J., Oliveros, E. & MacKay, A.: Advanced oxidation processes for organic contaminant destruction based on the Fenton reaction and related chemistry. *Crit. Rev. Environ. Sci. Tech.* 36 (2006), pp. 1–84.

Primo, O., Rivero, M.J. & Ortiz, I.: Photo-Fenton process as an efficient alternative to the treatment of landfill leachates. *J. Hazard. Mater.* 153 (2008), pp. 834–842.

Pupo Nogueira, R., Oliveira, M. & Paterlini, W.: Simple and fast spectrophotometric determination of H_2O_2 in photo-Fenton reactions using metavanadate. *Talanta* 66 (2005), pp. 86–91.

Puppo Nogueira, R., Trovó, A., da Silva, M., Villa, R. & Oliveira, M.: Fundamentos e aplicacoes ambientais dos procesos Fenton e photo-Fenton. *Quim. Nova* 30 (2007), pp. 400–408.

Reddy, D.H.K., Seshaiah, K., Reddy, A.V.R. & Lee, S.M.: Optimization of Cd(II), Cu(II) and Ni(II) biosorption by chemically modified *Moringa oleifera* leaves powder. *Carbohyd. Polym.* 88 (2012), pp. 1077–1086.

Schlegel, M.L. & Descostes, M.: Uranium uptake by hectorite and montmorillonite: A solution chemistry and polarized EXAFS study. *Environ. Sci. Technol.* 42 (2009), pp. 8593–8598.

Shah, V., Verma, P., Stopka, P., Gabriel, J., Baldrian, P. & Nerud, F.: Decolorization of dyes with copper(II)/organic acid/hydrogen peroxide systems. *Appl. Catal.* B: *Environ.* 46 (2003), pp. 287–292.

Singh, K. & Arora, S.: Removal of synthetic textile dyes from wastewaters: A critical review on present treatment technologies. *Crit. Rev. Environ. Sci. Technol.* 41 (2011), pp. 807–878.

Shinde, N.R., Bankar, A.V., Kumar, A.R. & Zinjarde, S.S.: Removal of Ni (II) ions from aqueous solutions by biosorption onto two strains of *Yarrowia lipolytica*. *J. Environ. Management* 102 (2012), pp. 115–124.

Soon, A.N. & Hameed, B.H.: Heterogeneous catalytic treatment of synthetic dyes in aqueous media using Fenton and photo-assisted Fenton process. *Desalination* 269 (2011), pp. 1–16.

Stylidi, M., Kondarides, D.I. & Verykios, X.E.: Pathways of solar light-induced photocatalytic degradation of azo dyes inaqueous TiO_2 suspensions. *Appl. Catal.* B: *Environ.* 40:4 (2003), pp. 271–286.

Sykora, J.: Photochemistry of copper complexes and their environmental aspects. *Coord. Chem. Rev.* 159 (1997), pp. 95–108.

Volesky, B.: Biosorption and me. *Water Res.* 41 (2007), pp. 4017–4029.

Wu, J., Li, B., Liao, J., Feng, Y., Zhang, D., Zhao, J., Wen, W., Yang, Y. & Liu, N.: Behaviour and analysis of Cesium adsorption on montmorillonite mineral. *J. Environ. Radioactiv*. 100 (2009), pp. 914–920.

Yip, A.C.-K., Lam, F.L.-Y. & Hu, X.: Novel bimetallic catalyst for the photo-assisted degradation of Acid Black 1 over a broad range of pH. *Chem. Eng. Sci.* 62 (2007), pp. 5150–5153.

Yipmantin, A., Maldonado, H.J., Ly, M., Taulemesse, J.M. & Guibal, E.: Pb(II) and Cd(II) biosorption on *Chondracanthus chamissoi* (a red alga). *J. Hazard. Mater*. 185 (2011), pp. 922–929.

Zhang,S., Liang, S., Wang, X., Long, J., Li, Z. & Wu, L.: Trinuclear iron cluster intercalated montmorillonite catalyst: Microstructure and photo-Fenton performance. *Catal. Today* 175 (2011), pp. 362–369.

Zhu, N., Gu, L., Yuan, H., Lou, Z., Wang, L. & Zhang, X.: Degradation pathway of the naphthalene azo dye intermediate 1-diazo-2- naphthol-4-sulfonic acid using Fenton's reagent. *Water Res.* 46 (2012), pp. 3859–3867.